J Sol-Gel Sci Technol (2017) 82:846–854
DOI 10.1007/s10971-017-4365-4

ORIGINAL PAPER: SOL-GEL AND HYBRID MATERIALS WITH SURFACE MODIFICATION FOR APPLICATIONS

The interaction of cellulose and montmorillonite in a hydrothermal process

Guangyu Yang[1] · Yinshan Jiang[1] · Xiaodong Yang[1] · Yuanjun Xu[1] · Shiding Miao[1] · Fangfei Li[1]

Received: 8 October 2016 / Accepted: 17 March 2017 / Published online: 27 March 2017

Abstract In this paper, the interaction of cellulose and montmorillonite in a hydrothermal process was discussed. The preparation of the composite was performed at 230 °C for different periods of time from 0.5 to 16 h. The hydroxypropyl methyl cellulose was set to 50 wt.% in the composite and multiple sets of data were compared. The samples were characterized by X-ray diffraction, Fourier transform infrared spectroscopy, scanning electron microscopy, thermogravimetry-differential thermal analysis, specific surface area and electric potential for evaluation of interactions. Hydrochar is a solid carbon-rich mixture produced from the hydrothermal carbonization of the cellulose. The cellulose can be adsorbed at the surface of montmorillonite. The pores of montmorillonite are partially blocked by the hydrochar. The state of the hydrochar has a significant effect on the order of montmorillonite. The zeta potential of the composite is mainly affected by hydrochar. In turn, the Fourier transform infrared spectroscopy results indicate that montmorillonite affects the hydrochar structure, and the thermal stability of hydrochar is improved. The experimental results show that the presence of hydrochar in the composite causes significant changes in surface properties and the interlayer structure. Meanwhile, montmorillonite plays a protective role on the hydrochar.

Graphical Abstract

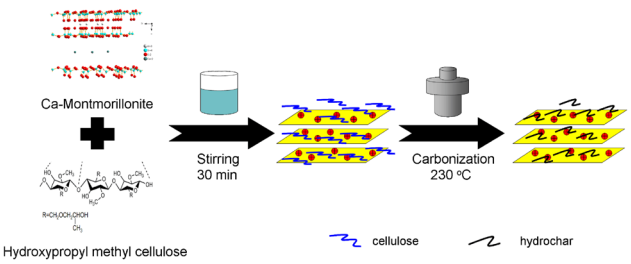

Keywords Montmorillonite · Hydrothermal carbonization · Cellulose · Clay minerals · Hydrochar

1 Introduction

Recently, the interaction of mineral and organic matter has attracted increasing interest in fields of soil science, geography, physics, chemistry, environmental science, etc. Montmorillonite (MMt) is one of the most important types of clay minerals, which has attractive features such as large surface area, swelling behavior, brilliant adsorption capacity, and ion exchange properties [1, 2]. Organic matters can not only be adsorbed by MMt, and be immobilized at the surface, but also can enter the interlayer spaces of MMt [3–5]. The MMt layers are negatively charged due to the isomorphous substitutions of Si^{4+} and/or Al^{3+} by cations of lower charges. The negative charge is always balanced by cations as Na^{+}, K^{+}, Li^{+}, and Ca^{2+} [6, 7]. However, these cations can be exchanged by organic ions, and more organic substances are able to be adsorbed by MMt due to its large specific surface area (SSA). Thus, the two dimensional MMt with

✉ Fangfei Li
lifangfei_jlu@163.com

[1] Key Laboratory of Automobile Materials, Ministry of Education, Department of Materials Science and Engineering, Jilin University, No. 5988 People's Avenue, Changchun 130025, People's Republic of China

expandable interlayer spaces has been used as an inorganic template to prepare high surface area of carbonous materials [8–10].

As is known, the natural carbonous materials were produced via in situ carbonization of biomass, which was always completed with the aid of clay minerals, e.g., the formation of soils. However, knowledge on the mutual effects between the biomass and clay minerals was less known. Usually, carbonization of biomass is carried out by pyrolysis. In recent years, hydrothermal carbonization (HTC) has been developed to transform labile biomass into a more stable end product (hydrochar) [11]. HTC is a process of heating biomass with presence of water at a temperature of 180–250 °C in a sealed vessel, and the hydrolysis is performed under a self-generated pressure [12]. The carbonizations are commonly found in the natural/geological processes. For example, the evolution of biomass was found in many sealed systems such as peats, soils, river marine sediments, biological origins of silica sedimentary rock-diatomite, and so on. The interaction of biomass and clay minerals at the interface is the main job to be investigated in clarifying this carbonization processes. More important this investigation helps to find a way of reducing CO_2 emission when the biomass was degraded in the pyrolytic carbonization process. The nature gives us an elegant example, i.e., the diatomite with higher content of bio-carbon was produced in a geological hydrolysis with burning of biomass [13, 14]. It was indicated that the carbon layer has an great influence on the phase transition and crystal structures of the diatomite [15]. The effect of clay on organic matter confirms that the minerals influence the transition of organic matter [16]. For example, the mineral-hydrochar nanocomposites have been developed through the HTC of natural biomass and layered minerals [17].

The interaction of biomass and clay minerals is widely existed in nature. However, the effects on the coexistence of mineral and biomass in HTC processes were less studied. In this paper, the interaction of hydroxypropyl methyl cellulose (HPMC) and MMt was discussed to research MMt surface effects in HTC processes. Therefore, we focus on the interaction of MMt and the cellulose under hydrothermal conditions. We combine the information that can be gathered with other known techniques, such as X-ray diffraction (XRD), SSA, thermal analysis, zeta potential and others. They are beneficial for the assessment of additional information regarding properties and structure of materials. The role of MMt in the evolution of the cellulose to hydrochar and the effect of HTC on the structure and surface properties of MMt are explored. The possible mechanism is proposed to provide a scientific basis for the preparation of new carbon materials and modified MMt.

2 Experimental procedures

2.1 Materials and chemicals

The bentonite which was composed mainly with MMt was supplied by Panshi, Jilin province, China. After purification via the Stocks method, the bentonite was found to contain a high percentage (90%) of Ca-MMt. Other minor mineral phases were identified as quartz, calcite, and feldspar. The chemical composition of the bentonite is listed as followed: 68.31% SiO_2, 16.39% Al_2O_3, 2.27% MgO, 2.27% Fe_2O_3, 0.53% K_2O, 1.94% CaO and 0.60% Na_2O. The cation exchange capacity is determined to be 80.45 meq/100 g. The biomass selected for this study is HPMC ($C_{12}H_{20}O_{10}$, FW:318.23) of analytical purity, which was purchased from YanXing Chemical, and used without further purification. The cellulose content is above 99.89 wt.%.

2.2 Preparation of MMt-hydrochar composite

The HTC of cellulose was carried out according to the following procedures. The MMt dispersion was prepared by adding 1.5 g of MMt powder in 20.0 mL DI water under vigorous stirring for 30 min. A portion of HPMC (1.5 g) was then added into the MMt dispersion, and the mixture was stirred at room temperature for another 30 min. The resultant mixture was transferred into a 50 mL Teflon-lined stainless steel autoclave, and was hydrothermally treated under autogenic pressure at 230 °C. To study the effects of hydrothermal time, a series of samples was prepared treating for 0.5, 1.0, 2.0, 4.0, 8.0, 12.0, and 16.0 h. Subsequently, the MMt-hydrochar composite was reclaimed by vacuum filtration followed by washing with DI water. The product was dried at 90 °C overnight. Finally the dried cake was ground to obtain MMt-hydrochar with particle size of 300 meshes.

2.3 Characterizations

The XRD measurements were carried out on the DX-2700 with a CuKα radiation at 35 kV and 25 mA. A Nicolet 380 Fourier transform infrared spectroscopy (FT-IR) spectrometer was used to collect FT-IR spectra. The zeta potential measurements were measured on a JS94J2 zeta apparatus. The thermo gravimetric analysis (TG) and differential thermal analysis (DTA) were performed on a HCT-3 TG/DTA system at a heating rate 10 °C/min from room temperature to a maximum temperature of 1000 °C in the atmosphere of air. The SSA was determined by using the Brunauer Emmett Teller method performed on a Micromeritics SSA-3600 analyzer. The scanning electron microscope (SEM) analyses were used to analyze the

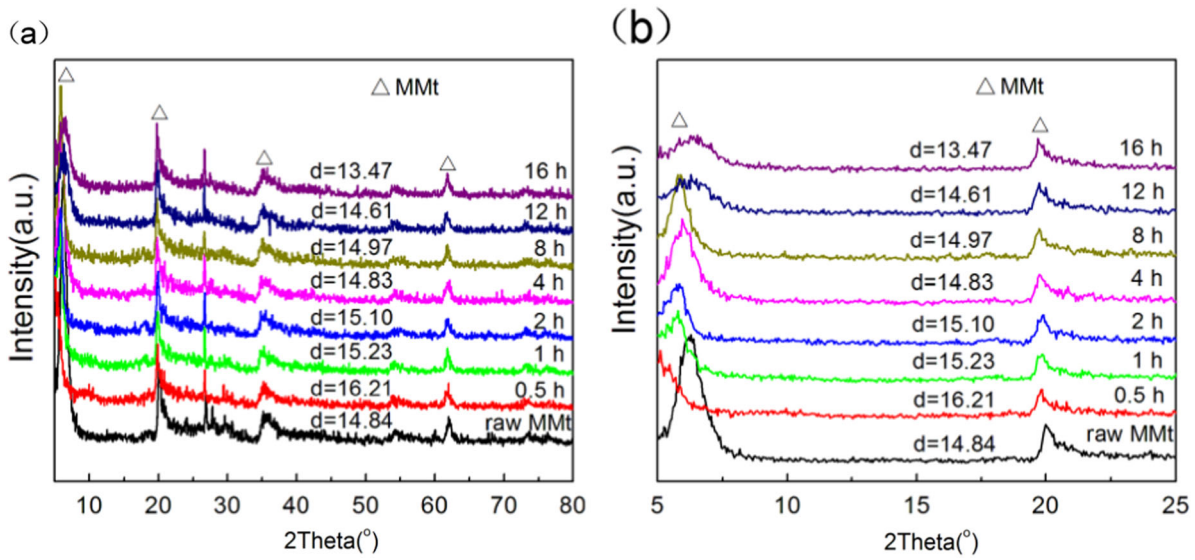

Fig. 1 XRD patterns of raw MMt and the MMt-derived composites treated at 230 °C for different periods of time **a** wide angle **b** narrow angle

micro-structure of the MMt composite samples, and the measurements were performed on a JSM-6700F apparatus.

3 Results and discussion

3.1 XRD analysis

The XRD patterns of the bentonite (raw MMt) and the MMt-derived composites treated for different periods of time (0.5, 1.0, 2.0, 4.0, 8.0, 12.0, and 16.0 h) are displayed in Fig. 1. The corresponding d_{001} values are also labeled in Fig. 1. The characteristic diffraction peaks were marked as triangles. The XRD spectra of the composite samples are basically identical to the raw MMt. Compared to the raw MMt, no new diffraction peaks of MMt-derived composites were generated. These results suggest that the cellulose carbonization does not change the structure of MMt, just changes the interlayer distance. The difference was found in the d_{001} values, which was caused by the cellulose carbonization. After hydrothermal treatment the color of MMt gradually changes from white to brownish black, indicating that the surface is coated by carbonaceous species [18]. With the development of HTC, the interlayer distance decreases from 1.621 to 1.347 nm. The interlayer distance of the MMt-derived composites decreases gradually with increasing retention time. From 0.5 to 4 h, the interlayer distance of the MMt-derived composites was found to have a decreasing trend. This can be explained by the loss of water from the interlayer due to hydrophobicity of carbonizing HPMC at the surface of MMt. The interlayer distance decreases from 1.621 to 1.483 nm, and the final $d_{001} =$ 1.483 nm of MMt composite is very close to that of the raw MMt. However, the interlayer distance increases to 1.497 nm for 8 h. After 8 h, the (001) reflection peak changes to be wide and low, which shows the layered structure of MMt is being destroyed by the HTC.

It clearly shows that the retention time has a significant effect on the order of MMt. The (001) reflection decreases in intensity with the increase of time after hydrothermal treatment. In addition, the water in the interlayer is discharged because of long retention time. This is reasoned by the replacement of hydrated exchangeable cations with hydrochar, depleting the exchangeable cations. This means that the carbonizing HPMC affects the interlayer distance of the composite greatly.

3.2 FT-IR analysis

Figure 2 shows the FT-IR spectra of raw MMt and the MMt-derived composites treated for different periods of time (0.5, 1.0, 2.0, 4.0, 8.0, 12.0, and 16.0 h). The FT-IR spectroscopy is further employed to determine the functional groups on the MMt-derived composites. The characteristic band of MMt at 3620 cm^{-1} is assigned to the vibration of Al–O–H, and the peaks at 3430 and 1630 cm^{-1} are stretching and bending vibrations of the H–O–H in absorbed water, respectively. The stretching vibration of Si–O–Si can be found at 1040 cm^{-1} [18]. The peak at 915 cm^{-1} is associated with the hydroxyl vibration of MMt. As shown in Fig. 2, there are two obvious absorption bands of MMt in low frequency region. The bands at 529 and 467 cm^{-1} related to the stretching vibration of Si–O–Al and bending vibration of Si–O–Si show increasing intensity for the MMt-derived composites [19]. The characteristic peaks corresponding to carbonaceous components can be also

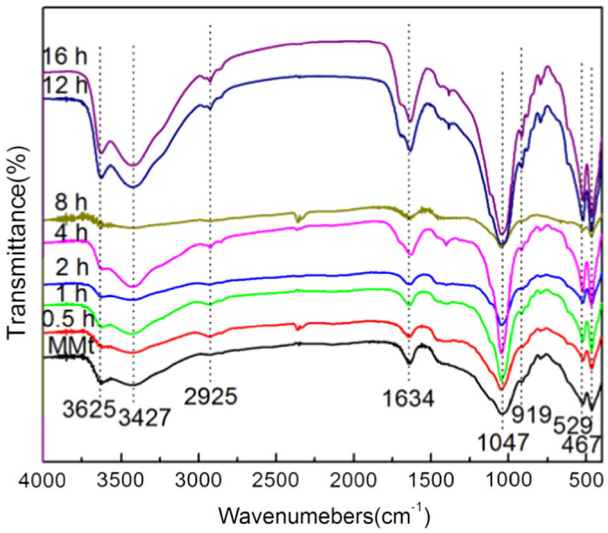

Fig. 2 FT-IR spectra of raw MMt and the MMt-derived composites treated at 230 °C for different periods of time

clearly visible. In relation to the MMt-derived composites, the HPMC is evidenced by the 2925 and 2895 cm^{-1} bands, related to asymmetric stretching of CH_3 and stretching of CH_2 groups from the silane [19].

Figure 3 shows the FT-IR spectra of raw HPMC treated at 230 °C for different periods of time (Fig. 3a) and the HPMC of MMt-derived composites in toluene solution (Fig. 3b). The small molecules can be extracted by toluene. There are three kinds of absorption peaks for the HPMC in the infrared spectrum. The band at 1705 cm^{-1} is assigned to C=O stretching vibration, and the skeletal C=O stretching vibration is at 1025 cm^{-1}. And there are several bands which reveal that aromatization processes take place during HTC. The presence of aromatic rings is also evidenced by the band at 1620 cm^{-1}, attributed to C=C vibrations [20], and the band at 799 cm^{-1} is assigned to aromatic C–H out-of-plane bending vibration from the aromatic ring [21]. The band at 1510 cm^{-1} originates from the aromatic skeletal C=C vibration of benzene [22]. These vibrations are present in the spectrum of raw cellulose in Fig. 3a, which represents the conversion from cellulose to hydrochar [23]. But the band at 1510 cm^{-1} is not observed in Fig. 3b.

These hydrochar materials also possess aliphatic structure, as can be deduced from the bands at 2815–3000 cm^{-1}, which correspond to stretching vibrations of aliphatic C–H [19]. In Fig. 3b, the bands at 1465 and 1401 cm^{-1} are assigned to C–H stretching vibrations implying that the aliphatic compounds are present [24]. However, they are not observed in the spectra of raw hydrochar samples in Fig. 3a. The main body of aliphatic chain enters into the interlayer of expansive MMt, which causes the interaction of methylene and oxygen in the bottom of silicon oxygen tetrahedral [25]. Therefore, the MMt plays a protective role on hydrochar, and the stability of hydrochar is obviously enhanced. In addition to the above, other peaks show similarity to those of raw HPMC. The findings clearly demonstrate that the hydrochar is strongly influenced by MMt.

3.3 TG/DTA analysis

The TG/DTA thermograms of the MMt-derived composites treated at 230 °C are shown in Fig. 4. The mass loss of MMt-derived composites can be divided into three stages. The first stage is mainly the loss from 50 to 170 °C, which is caused by the removal of physically adsorbed water in the interlayer. The second one is mainly the burn and decomposition of hydrochar from 300 to 500 °C. In this range, the burn and decomposition lead to the formation of primary hydrochar, volatiles, and gases [26]. This phenomenon can be explained by the extended breaking down of C–H and C–C bonds, which results in continuous hydrochar devolatilisation [27]. The decomposition undergoes a slow progress after 350 °C since the rest of the hydrochar is decomposed [28, 29]. The first peak occurs at 340 °C due to the pyrolysis, whereas the second one is originated from char oxidation at 490 °C [30]. The third stage is attributed to the dehydroxylation from 600 to 700 °C. The property of MMt is completely destroyed at this stage.

The mass loss of the composite is much lower than raw MMt at 90.9 °C because of the reduction of MMt content. The second stage of mass loss (300–500 °C) accompanies with three exothermic DTA peaks at 313, 393, and 455 °C. It can be assigned to the removal for burn and decomposition of hydrochar. The exothermic peaks at around 313.3 and 455.2 °C are visible after 2 h, which can be attributed to the heat transfer of the HPMC cut off by MMt. When the conversion from HPMC to hydrochar has finished, barrier effect of the MMt is meaningless. It shows MMt has an important influence on the heat transfer of HPMC instead of hydrochar. With the development of HTC, the decomposition temperature of hydrochar raises at second stage. The maximum decomposition temperature of the MMt-derived composites reaches the highest at 16 h. The TG/DTA results indicate that the thermal stability of hydrochar is improved.

The mass loss between 200 and 500 °C is 31.2% for 4 h, 26.4% for 8 h, 22.5% for 12 h, 23.9% for 16 h, respectively. The mass loss of the MMt-derived composites for 4 and 8 h is the fastest at second stage. Because the hydrochar contain a large number of aromatic ring structures and oxygen functional groups that are hydrophilic [31], which is in good agreement with the results obtained by FT-IR. The oxygen functional groups of the hydrochar decrease with raising the temperature. And the structure becomes more and more compact, which is in good agreement with the results

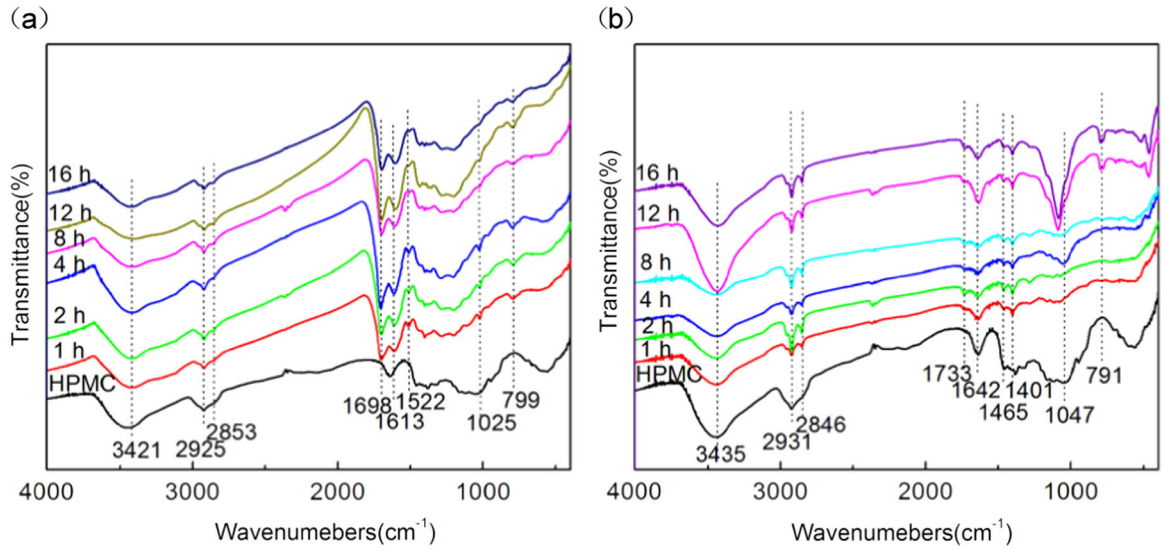

Fig. 3 FT-IR spectra of **a** raw HPMC treated at 230 °C for different periods of time **b** the HPMC of the MMt-derived composites in toluene solution

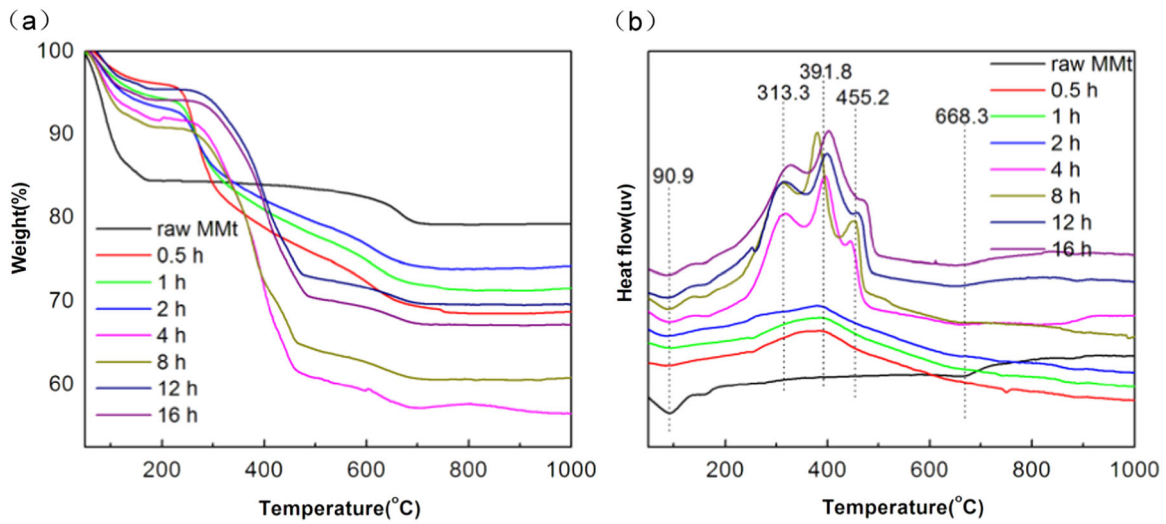

Fig. 4 TG (**a**) and DTA (**b**) patterns of the MMt-derived composites treated at 230 °C for different periods of time

obtained by SEM. Therefore, the mass loss of the MMt-derived composites is fewer after 12 h.

The composite and HPMC treated at 230 °C for 4 h are present in Fig. 5. Exothermic peak and heat release are significantly different. The mass loss of the composite is from 300 to 500 °C, accompanied with three exothermic DTA peaks at 314, 395, and 445 °C. The mass loss of HPMC is 100% at 550 °C, accompanied with three exothermic DTA peaks at 265, 333, and 498 °C. Moreover, the weight loss rate is slightly different. The HPMC from composite burns more slowly because of the heat prevent by MMt. However, the final mass loss of the composite is less than 50%. The hydrochar loses a part of mass because of the dehydrogenation and deoxygenation in the process of carbonization. It leads the declining mass proportion for HPMC in the composite.

3.4 Zeta analysis

The effects of raw HPMC, raw MMt and the MMt-derived composites on the zeta potential of deionized water for different periods of time are shown in Fig. 6. It could be seen that the zeta potential of the MMt-derived composites decreases greatly with increasing retention time. It means that the longer retention time, the more surface charges of the MMt-derived composites generate. The HPMC and MMt particles carry negative electric charges. The HTC of HPMC at MMt surface enhances the density of negative

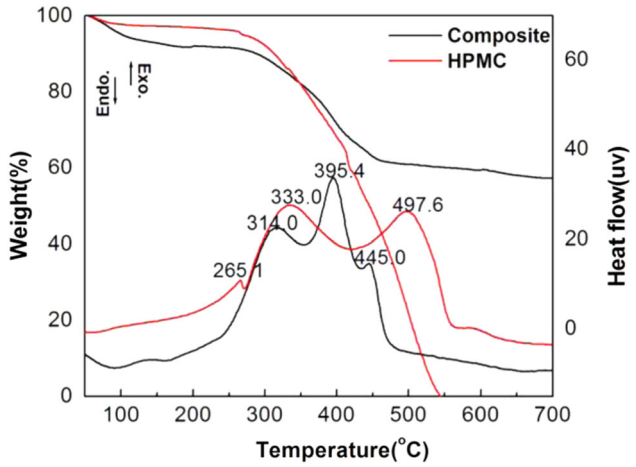

Fig. 5 TG-DTA pattern of the MMt-derived composites and HPMC treated at 230 °C for 4 h

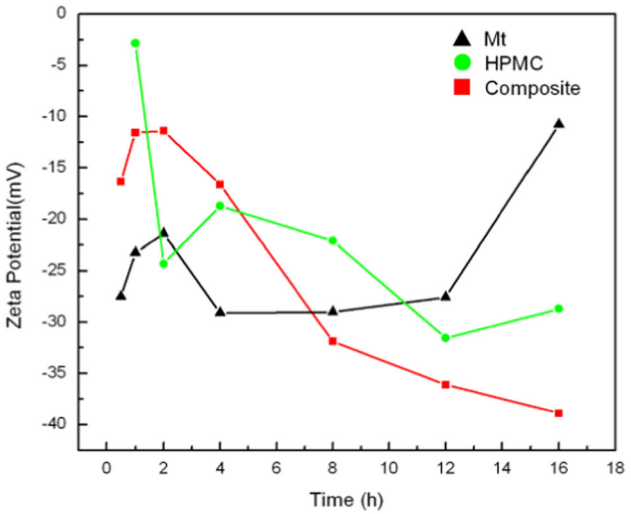

Fig. 6 The effects of raw HPMC, raw MMt and the MMt-derived composites treated at 230 °C for different periods of time on the zeta potential

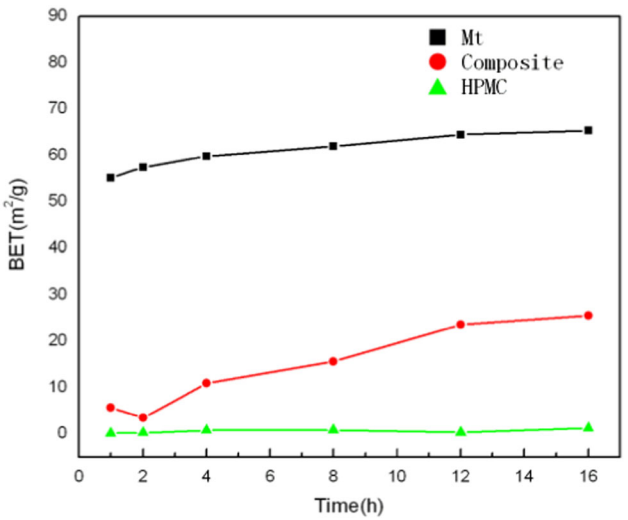

Fig. 7 The SSA of raw MMt, the MMt-derived composites and raw HPMC treated at 230 °C for different periods of time

electric charge. Thus the electrostatic repulsive interaction of MMt and HPMC particles increases, the synergetic and steric effects enhance the stability of the composite.

The zeta potential of the MMt-derived composites increases within 2 h. It is indicated that the coalescence of the particles do take place due to the electrostatic attraction interaction. It decreases the difficulty for the MMt and hydrochar particles to approach toward each other [32]. On the other hand, the zeta potential decreases when the retention time increases from 2 to 8 h, which is related to the HTC. It can be seen that the zeta potential decreases sharply within 8 h. With the further increase of the retention time, the zeta potential is to stabilize, which is attributed to the adsorption of HPMC at the surface of MMt is mainly carbonized. After 8 h, the zeta potential decreases slowly, which illustrates that less HPMC is carbonizing. Within 4 h, the trend of the composite is consistent with MMt, which illustrates MMt plays a leading role. After 4 h, the composite basically follows HPMC, which illustrates HPMC makes important effects after HTC.

The negative charge increases with the development of HTC. The adsorption of HPMC can reach equilibrium after the conversion from HPMC to hydrochar, resulting in a constant value of zeta potential. Thus, the MMt and hydrochar particles are simultaneously present in the deionized water to cause the difficulty of the MMt-derived composites coalescence. Although the carbonization of HPMC can increase the negative electric charge through the formation of hydrochar, it can also compress the diffuse double layer of MMt to increase the zeta potential after 8 h.

3.5 SSA analysis

The SSA of raw MMt, the MMt-derived composites and raw HPMC for different periods of time are shown in Fig. 7. The SSA of raw MMt increases from 48.8 to 65.4 m^2/g, while the HPMC changes little over time. Compared to the raw MMt, the SSA of MMt-derived composites are lower on the whole, which is probably because the pores of MMt are partially blocked by the carbonaceous particles in the HTC process [18]. This result is in accordance with that of SEM analysis.

3.6 SEM analysis

The SEM images are showing the changes in morphologies of the composite for different retention time. It reveals the MMt has a rough surface that is a considerable potential for

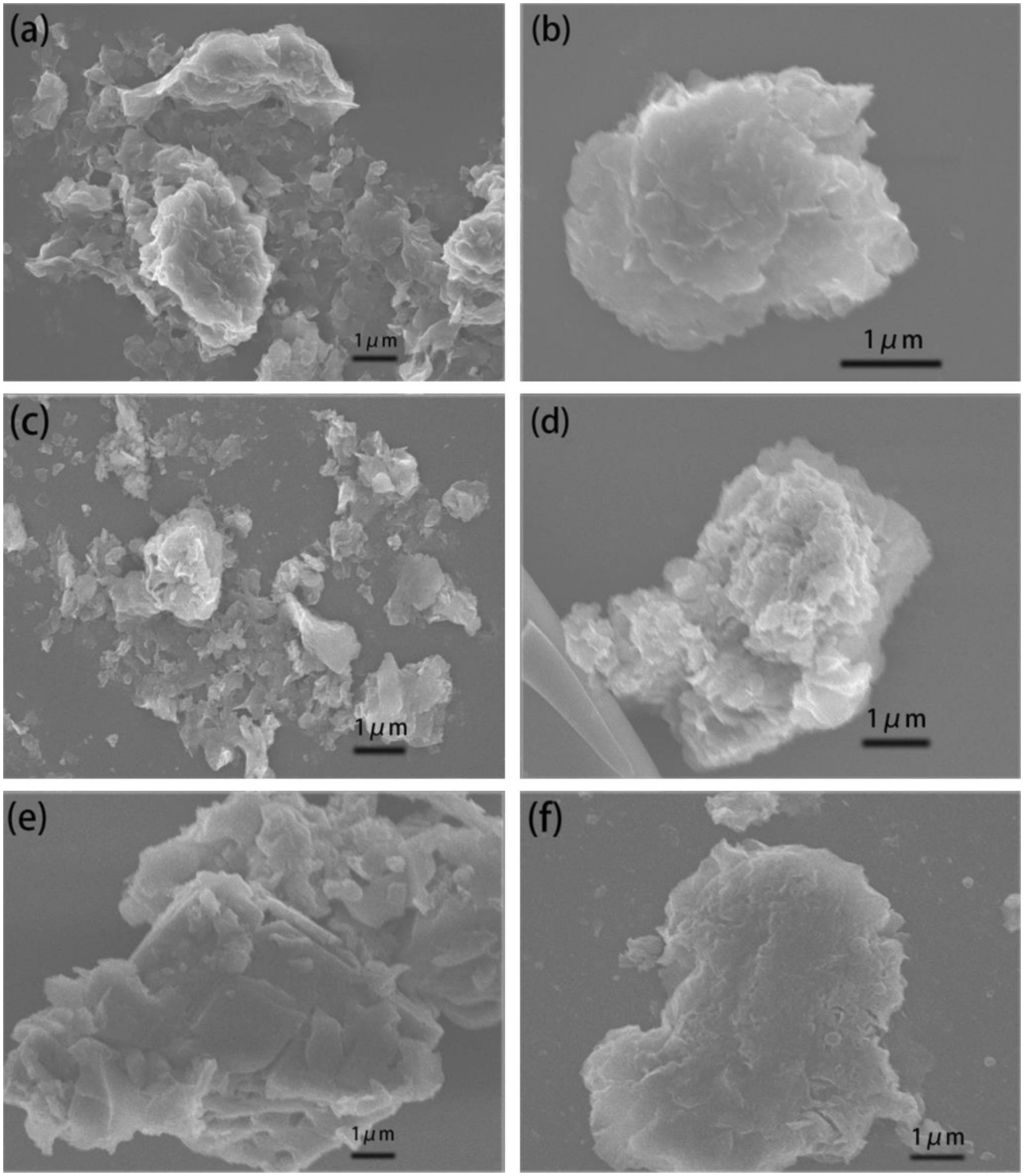

Fig. 8 SEM microphotographs of the MMt-derived composites treated at 230 °C for different periods of time **a** 1 h **b** 2 h **c** 4 h **d** 8 h **e** 12 h **f** 16 h

the adsorption of HPMC (Fig. 8a and b) [33]. The MMt exhibits a typical layered structure with a smooth surface (Fig. 8a and b). The MMt-derived composites for longer retention time directly or slowly yield a tightly packed pattern in SEM micrographs (Fig. 8c and d) [34]. These tightly packed structures and flower-like pores may result from the carbonization of HPMC, which causes a change at the surface charge of the particles [35]. The morphology and size variation of the MMt-derived composites particles are explored as a function of interaction time after the HTC

of HPMC at the surface. At the initial stage of HTC process, the morphology of MMt-derived composites displays typical multi-layered shape. While, after 8 h HTC treatment, the conversion process from HPMC to hydrochar obscures the boundary space between MMt layers, which thicken the MMt-derived composites. Thus the MMt-derived composites particles are irregular in shape and mostly present in aggregates because of the hydrochar (Figs. 8e and f).

4 Conclusions

In conclusion, the MMt-hydrochar composites are successfully synthesized in the aqueous dispersion. The state of HPMC has a significant effect on the order of MMt. With the development of HTC, the interlayer distance decreases from 1.621 to 1.347 nm. The HPMC can be adsorbed at the surface of MMt. The pores of MMt are partially blocked by the hydrochar in the HTC process. The dispersive properties of the composite improve over hydrothermal time. The zeta potential of the composite is mainly affected by MMt when HPMC is not completely carbonized. Moreover, the MMt plays a protective role on the hydrochar and its thermal stability is enhanced. The MMt has an important influence on the heat transfer of HPMC instead of hydrochar. The presence of hydrochar in the composite causes significant changes in surface properties and the interlayer structure. Meanwhile, MMt plays a protective role on the hydrochar.

Acknowledgements We acknowledged the funding support from the financial support of the National Natural Science Foundation of China (NSFC, grant No.41472035 and grant No.51304080).

Conflict of Interest The authors declare that they have no competing interest.

References

1. Khaorapapong N, Ontam A, Khemprasit J et al. (2009) Formation of MnS- and NiS-montmorillonites by solid–solid reactions. Appl Clay Sci 43(2):238–242
2. Khaorapapong N, Ogawa M (2007) Solid-state intercalation of 8-Hydroxyquinoline into Li(I)-, Zn(II)- and Mn(II)-montmorillonites. Appl Clay Sci 35(1–2):31–38
3. Kennedy MJ, Pevear DR, Hill RJ (2002) Mineral surface control of organic carbon in black shale. Science 295 (5555):657–660
4. Yariv S, Lapides I (2005) The use of thermo-XRD-analysis in the study of organo-smectite complexes Robert Mackenzie memorial lecture. J Therm Anal Calorim 80(1):11–26
5. Lu L, Cai J, Liu W et al. (2012) Infra-red emission spectroscopy study of thermal evolution of organic matter bound by clay minerals in muddy hydrocarbon source rocks. Pet Geol Exp 34 (2):215–222
6. Banković P, Milutinović-Nikolić A, Mojović Z et al. (2013) Synthesis and characterization of bentonites rich in beidellite with incorporated Al or Al–Fe oxide pillars. React Kinet Catal Lett 165 (165):247–256
7. Ohtsuka K (1997) ChemInform abstract: preparation and properties of two-dimensional microporous pillared interlayered solids. Chem Mater 9(10):2039–2050
8. Sonobe N, Kyotani T, Tomita A (1990) Carbonization of polyfurfuryl alcohol and polyvinyl acetate between the lamellae of montmorillonite. Carbon N Y 28(4):483–488
9. Bakandritsos A, Steriotis T, Petridis D (2004) High surface area montmorillonite−carbon composites and derived carbons. Chem Mater 16(8):1551–1559
10. Jiang G, Zhou CH, Xia X et al. (2010) Controllable preparation of graphitic carbon nitride nanosheets via confined interlayer nanospace of layered clays. Mater Lett 64(24):2718–2721
11. Wiedner K, Naisse C, Rumpel C et al. (2013) Chemical modification of biomass residues during hydrothermal carbonization—what makes the difference, temperature or feedstock? Org Geochem 54(1):91–100
12. Libra JA, Ro KS, Kammann C et al. (2011) Hydrothermal carbonization of biomass residuals: a comparative review of the chemistry, processes and applications of wet and dry pyrolysis. Biofuels 2(1):71–106
13. Bing X, Jiang YS, Yang DF et al. (2011) Carbonization treatment of diatomite with high ignition loss and reinforcement of natural rubber. J Fish Biol 47(sA):127–144
14. Zheng Q, Bing X, Shaonan XU et al. (2013) Carbonization treatment and adsorption properties of diatomite with organics. Food Sci Biotechnol 24(5):1679–1685
15. Ying G, Xie YC (2010) Influence of carbon on phase transformation of oxides in carbon/oxide composites. Acta Phys Chim Sin 26(7):1887–1892
16. Wang X, Cai J, Bao Y (2006) Catalysis of clay mineral to organic matter in hydrocarbon genesis. Mar Orig Pet Geol 11:27–38
17. Wu LM, Tong DS, Li CS et al. (2015) Insight into formation of montmorillonite-hydrochar nanocomposite under hydrothermal conditions. Appl Clay Sci 119:116–125
18. Zhang R, Chen C, Li J et al. (2015) Preparation of montmorillonite@carbon composite and its application for U(VI) removal from aqueous solution. Appl Surf Sci 349:129–137
19. Romanzini D, Piroli V, Frache A et al. (2015) Sodium montmorillonite modified with methacryloxy and vinylsilanes: influence of silylation on the morphology of clay/unsaturated polyester nanocomposites. Appl Clay Sci 114:550–557
20. Zhang Z, Ke W, Atkinson JD et al. (2012) Sustainable and hierarchical porous Enteromorpha prolifera, based carbon for CO_2, capture. J Hazard Mater 229-230(5):183–191
21. Guo S, Dong X, Wu T et al. (2015) Characteristic evolution of hydrochar from hydrothermal carbonization of corn stalk. J Anal Appl Pyrolysis 116:1–9
22. Schwanninger M, Rodrigues JC, Pereira H et al. (2004) Effects of short-time vibratory ball milling on the shape of FT-IR spectra of wood and cellulose. Vib Spectrosc 36(1):23–40
23. Düdder H, Wütscher A, Stoll R et al. (2015) Synthesis and characterization of lignite-like fuels obtained by hydrothermal carbonization of cellulose. Fuel 171:54–58
24. Durig JR, Zhu X, Guirgis GA et al. (2003) Infrared and raman spectra, conformational stability, ab initio calculations of structure and vibrational assignment of 4-fluoro-1-pentyne. J Mol Struct 657(1–3):271–289
25. Lu L, Cai J, Liu W et al. (2012) Infra-red emission spectroscopy study of thermal evolution of organic matter bound by clay minerals in muddy hydrocarbon source rocks. Pet Geol Exp 34 (2):215–222
26. Demirbas A (2004) Effects of temperature and particle size on bio-char yield from pyrolysis of agricultural residues. J Anal Appl Pyrolysis 72(2):243–248

27. Koufopanos CA, Lucchesi A, Maschio G (1989) Kinetic modelling of the pyrolysis of biomass and biomass components. Can J Chem Eng 67(67):75–84
28. Fisher T, Hajaligol M, Waymack B et al. (2002) Pyrolysis behavior and kinetics of biomass derived materials. J Anal Appl Pyrolysis 62(2):331–349
29. Wongsiriamnuay T, Tippayawong N (2010) Non-isothermal pyrolysis characteristics of giant sensitive plants using thermogravimetric analysis. Bioresour Technol 101(14):5638–5644
30. Düdder H, Wütscher A, Stoll R et al. (2015) Synthesis and characterization of lignite-like fuels obtained by hydrothermal carbonization of cellulose. Fuel 171:54–58
31. Wang J, Shi L, Gao Y et al. (2013) Structure evolution of char obtained from hydrothermal treatment of glucose. Trans Chin Soc Agric Eng 29(7):191–198
32. Li F, He W, Sun D et al. (2015) Effect of sodium-montmorillonite particles on the stability of oil droplets in produced water from alkali/surfactant/polymer flooding. J Clean Prod 104:468–474
33. Rostami MR, Kaya M, Gür B et al. (2015) Photophysical and adsorption properties of pyronin B in natural bentonite clay dispersion. Appl Surf Sci 359:897–904
34. Tomul F (2015) The effect of ultrasonic treatment on iron–chromium pillared bentonite synthesis and catalytic wet peroxide oxidation of phenol. Appl Clay Sci 120:121–134
35. Anirudhan TS, Bringle CD, Rijith S (2010) Removal of uranium (VI) from aqueous solutions and nuclear industry effluents using humic acid-immobilized zirconium-pillared clay. J Environ Radioact 101(3):267–276